Macromolecules

Article

pubs.acs.org/Macromolecules

Ring Polymer Dynamics Are Governed by a Coupling between Architecture and Hydrodynamic Interactions

Kai-Wen Hsiao, Charles M. Schroeder, and Charles E. Sing*

Department of Chemical and Biomolecular Engineering, University of Illinois Urbana−Champaign, Urbana, Illinois 61801, United States

ABSTRACT: The behavior of linear polymer chains in dilute solution flows has an established history. Polymers often possess more complex architectures, however, such as branched, dendritic, or ring structures. A major challenge lies in understanding how these nonlinear chain topologies affect the dynamic properties in nonequilibrium conditions, in both dilute and entangled solutions. In this work, we interrogate the single-chain dynamics of ring polymers using a combination of simulation, theory, and experiment. Inspired by recent experimental results by Li et al., we demonstrate that the presence of architectural constraints has surprising and pronounced effects on the dynamic properties of polymers as they are driven out of equilibrium. Ring constraints lead to two behaviors that contrast from linear chains. First, the coil−stretch transition occurs at larger values of the dimensionless flow strength (Weissenberg number) compared to linear chains, which is driven by coupling between intramolecular hydrodynamic interactions (HI) and chain architecture. Second, a large loop conformation is observed for ring polymers in extensional flow at intermediate to large Weissenberg numbers, and we show that this open loop conformation is driven by intramolecular HI. Our results reveal the emergence of new paradigms in chain architecture−hydrodynamic coupling that may be relevant for solution-based processing of polymeric materials and could provide new opportunities for precise flow-based polymer conformation control to guide material properties.

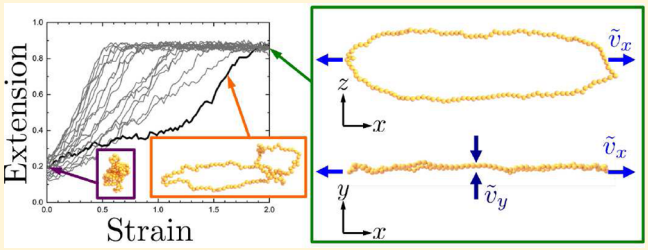

INTRODUCTION

Ring polymers are intensely studied in polymer physics, primarily due to their status as a model system for understanding the role of chain topology.[1−3] Circular (or ring) polymers provide the opportunity to probe some of the most fundamental features of long-chain macromolecules. For example, the absence of chain ends leads to compelling questions with regards to entanglements: how does an entangled melt of rings relieve stress, given the absence of free chain ends? How does this affect the flow properties of ring-based materials? Over the past several years, a large amount of literature has been devoted to these questions.[1,4−8] The essence of the question lies in understanding how a polymer that has similar local random walk statistics compared to a linear polymer is altered by the constraint that the overall chain must return to its starting point.[1−3]

These fundamental questions in ring polymer dynamics are typically considered in the context of concentrated systems;[1,4−8] however, recent work has begun to probe the dynamic behavior of single ring polymer chains in dilute solution.[9−11] Such systems are motivated by the success of single-chain dynamics, which has informed polymer dynamics for a half century. This field stemmed from pioneering work by Rouse and Zimm that established the language of polymer relaxation and dynamics in the linear regime.[12,13] Moving forward, additional work by others including Peterlin and De Gennes[14,15] established the theoretical principles of how polymers stretch in fluid flows. The fundamental competition relevant for nonequilibrium polymer dynamics is between hydrodynamic flow fields that stretch a polymer and the entropic forces that drive a polymer to relax back to a random coil. This competition leads to a coil−stretch transition in extension-dominated flows and a weaker second-order transition in simple shear flows.[14,15] The details of this transition are sensitive to hydrodynamic interactions (HI) between polymer segments in solution.[13] In essence, intramolecular HI leads to hydrodynamic screening in the coiled state, with hydrodynamic friction or drag increasing as a polymer chain unravels in flow. This conformation-dependent drag ultimately gives rise to a first-order-like coil-to-stretch transition for chains in elongation flows.[15,16] From this perspective, the single-chain problem has contributed substantially to our understanding of polymer dynamics and rheology, both as a limiting case that informs concentrated polymer dynamics and as a technologically relevant physical description of polymers useful for solution processing or for flow-based polymer manipulation.[11,17,18]

Bulk rheological and rheooptical techniques such as birefringence and light scattering have provided a wealth of information regarding polymer chain dynamics.[15] Bulk-level techniques, however, can only indirectly infer molecular features of polymer stretching dynamics by measuring bulk

Received: October 29, 2015
Revised: February 11, 2016
Published: February 19, 2016

DOI: 10.1021/acs.macromol.5b02357
Macromolecules 2016, 49, 1961−1971

materials properties. In recent years, single molecule fluorescence microscopy has enabled direct imaging of polymer chains and visualization of dynamic conformational evolution in nonequilibrium fluid flow.[17,18] This approach has led to the ability to directly probe the fundamental predictions of polymer dynamics: single-chain diffusivity,[19] conformational relaxation,[20−22] flow-driven chain stretching in both elongation and shear flows,[16,23−25] chain tumbling,[26] confinement effects,[27] and conformational chain hysteresis predicted decades earlier.[16] New experimental and theoretical efforts have focused on nonlinear architectures,[10,11,22] collapsed polymers,[28−31] knotted polymers,[32,33] and nondilute solutions.[11]

Compared to linear chains, ring polymers have received less attention in the context of single-chain dynamics,[34,35] despite substantial literature considering their melt properties.[1,4−8] Nevertheless, the fundamental question of topological constraints in ring polymers remains important in the case of single-chain dynamics. This article exposes surprising results that arise in the elongational flow-induced stretching of ring polymers in strong flows.[9] In particular, we observe a coupling between chain architecture of ring polymers and intramolecular HI between polymer segments, which becomes highly nontrivial and leads to changes in the critical flow strength at the onset of the coil−stretch transition. Interestingly, these interactions also lead to a transient looped conformation in the fully stretched polymer ring. This work addresses recent observations in the literature regarding ring polymers in dilute solution flows[9] and suggests that the coupling between hydrodynamics and chain connectivity is an area with rich phenomenology in the context of polymers with nonlinear topologies.

METHODS

Simulation. We use standard Brownian dynamics (BD) methods to model a single ring polymer in an implicit solvent undergoing an elongational flow.[17,28,29] The model considers the polymer chain to be composed of N beads of index i at positions $\mathbf{r}_i$. We follow the trajectory of these beads in a potential U given by

$$\tilde{U} = \frac{\tilde{\kappa}}{2}\sum_{i=1}^{N-1}(\tilde{r}_{i+1,i}-2)^2 + \frac{\tilde{\kappa}}{2}(\tilde{r}_{1,N}-2)^2 + \tilde{u}\sum_{ij}\left[\left(\frac{2}{\tilde{r}_{i,j}}\right)^{12} - 2\left(\frac{2}{\tilde{r}_{i,j}}\right)^{6}\right] \quad (1)$$

where $\tilde{r}_{i,j}$ is the dimensionless distance between beads i and j, and $\tilde{u}$ is the depth of the Lennard-Jones potential between spatially adjacent beads. We use a Hookean spring constant $\tilde{\kappa}$ = 200 between connecting beads, which is sufficiently strong such that the model essentially acts as a bead−rod model. In all simulations, the bonds stretch no more than 10−15% of their equilibrium length. This occurs only in very high flow rates, with most simulations deviating much less than 5−10%. This minimal stretching, along with the finite size of the beads, renders chain crossing essentially impossible. All values have been normalized (denoted by a tilde): distances are in units of the bead radius a, energies are in units of the thermal energy k_BT, and time is in units of the single bead diffusion time $\tau_D = (6\pi\eta a^3)/(k_BT)$ where η is the solvent viscosity. We primarily use $\tilde{u}$ = 0.35, which is the Θ-condition for polymers.[28] Good solvents are also considered, with $\tilde{u}$ = 0.10.

Chain dynamics are governed by the Langevin equation:[28]

$$\frac{\partial\tilde{\mathbf{r}}_i}{\partial\tilde{t}} = \tilde{\mathbf{\Gamma}}\cdot(\tilde{\mathbf{r}}_i - \tilde{\mathbf{r}}_{com}) - \sum_j \tilde{\mu}_{ij}\nabla_{\tilde{\mathbf{r}}_j}U + \boldsymbol{\xi}_i(\tilde{t}) \quad (2)$$

where the mobility matrix μ_{ij} accounts for the hydrodynamic interactions between particles i and j. We consider two behaviors for this matrix: freely draining (FD) and hydrodynamically interacting (HI). FD considers no hydrodynamic coupling between beads, and the only hydrodynamic force is the drag on a given bead. Therefore, the FD case gives $\tilde{\mu}_{ij} = \delta_{ij}\mathbf{I}$, where δ_{ij} is the Kronecker delta and $\mathbf{I}$ is the identity matrix. The inclusion of HI considers hydrodynamic coupling between the beads. In this case, we use the Rotne−Prager−Yamakawa tensor for $i \neq j$:[36,37]

$$\tilde{\mu}_{ij} = \begin{cases} \frac{3}{4\tilde{r}_{i,j}}\left(\left(1+\frac{2}{3\tilde{r}_{ij}^2}\right)\mathbf{I} + \left(1-\frac{2}{\tilde{r}_{ij}^2}\right)\frac{\tilde{\mathbf{r}}_{ij}\tilde{\mathbf{r}}_{ij}}{\tilde{r}_{ij}^2}\right) & \tilde{r}_{ij} \geq 2 \\ \left(1-\frac{9\tilde{r}_{ij}}{32}\right)\mathbf{I} + \frac{3}{32}\frac{\tilde{\mathbf{r}}_{ij}\tilde{\mathbf{r}}_{ij}}{\tilde{r}_{ij}} & \tilde{r}_{ij} < 2 \end{cases} \quad (3)$$

A Cholesky decomposition of this tensor is used to calculate the random velocity ξ_i, in order to satisfy the fluctuation−dissipation theorem $\langle\xi_i(t)\xi_j(t')\rangle = 2k_BT\mu_{ij}\delta(t-t')$.[28] We note that the $i = j$ case uses the Stokes friction $\tilde{\mu}_{ii} = \mathbf{I}$.[28] The term in eq 2 that includes the dimensionless velocity gradient tensor $\tilde{\mathbf{\Gamma}}$ is the undisturbed velocity field due to the applied fluid flow. In the case of planar elongational flow, we use

$$\tilde{\mathbf{\Gamma}} = \begin{bmatrix} \tilde{\dot{\epsilon}} & 0 & 0 \\ 0 & -\tilde{\dot{\epsilon}} & 0 \\ 0 & 0 & 0 \end{bmatrix} \quad (4)$$

where the strain rate is nondimensionalized by the diffusion time of a single bead, yielding the bead Peclet number $\tilde{\dot{\epsilon}}$. Figure 1 illustrates the geometry of a planar elongational flow. In the case of extensional flow, we also define a dimensionless flow strength by the Weissenberg number $Wi = \tilde{\dot{\epsilon}}\tilde{\tau}_R$, where $\tilde{\tau}_R$ is the dimensionless longest relaxation time of the polymer (see below). Simulations integrate eq 2 with a time step of $\Delta\tilde{t} = (2-5)\times10^{-4}$ and are generally run for between $(20-100)\times10^6$ time steps.

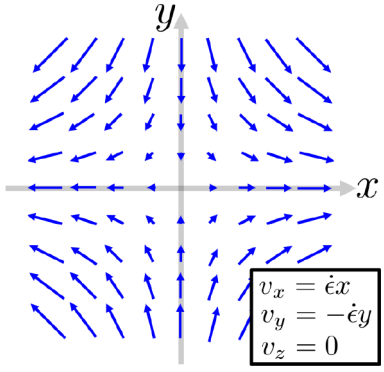

Figure 1. This article considers a planar elongational flow. This flow geometry consists of a principal axis of extension (in this case, x) and a principal axis of compression (y), while the z-direction has no flow.

DOI: 10.1021/acs.macromol.5b02357
Macromolecules 2016, 49, 1961−1971

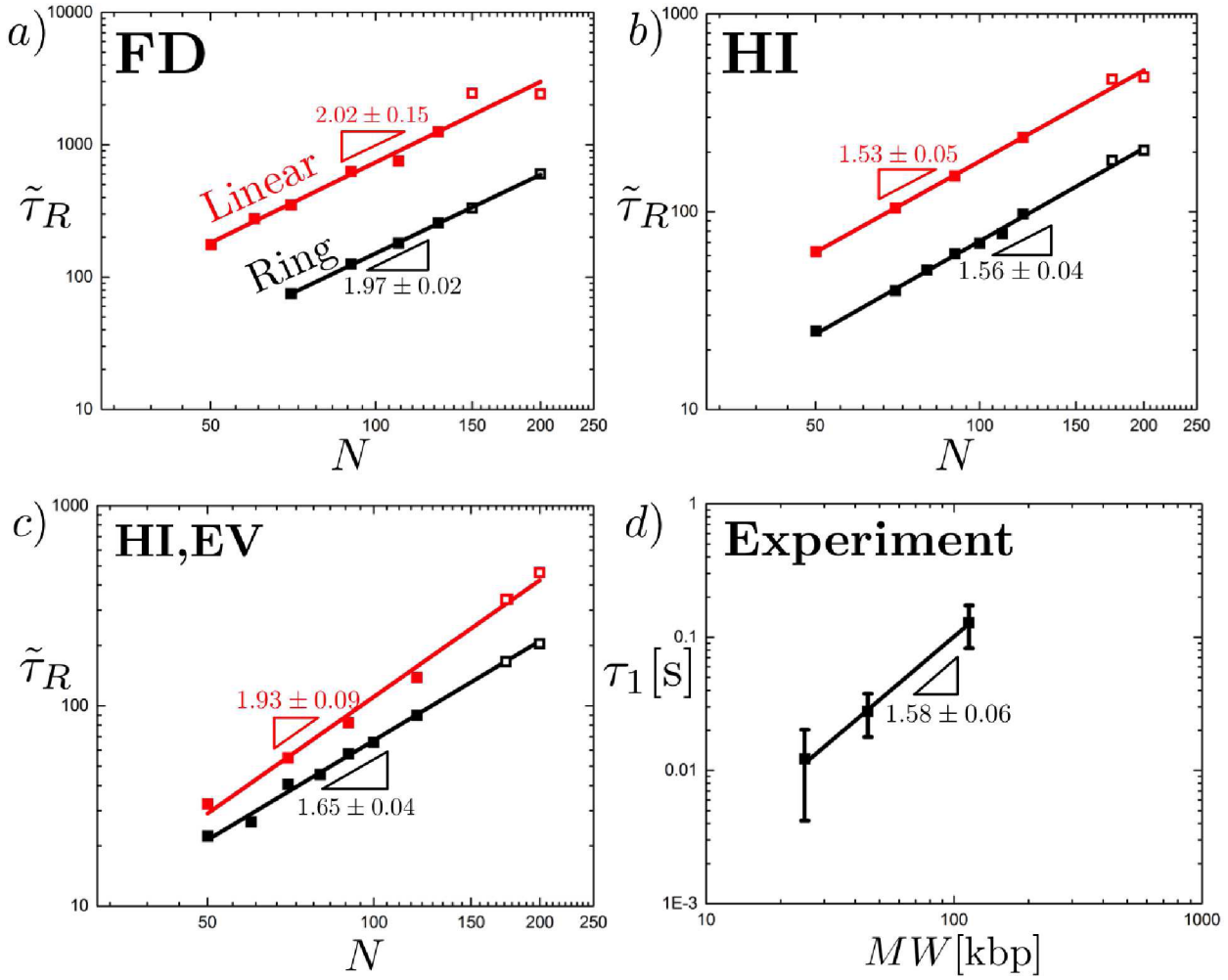

Figure 2. Relaxation time τ_R as a function of chain length N for ring and linear chains, determined either from the relaxation of a stretched polymer (solid symbols) or from the time correlation function of polymer dimensions (open symbols, see text for details). (a) Longest relaxation time for both linear chains and rings in the FD approximation in Θ-solvent. The observed scaling $\tau_R \sim N^2$ is expected for Rouse dynamics. The difference in the best fit intercepts is $\Delta \log \tilde{\tau}_R \approx 0.60 \pm 0.31$, consistent with the factor of 4 difference between the relaxation times for the ring and linear chains ($\log 4 = 0.6$).[12,38,39] (b) Longest relaxation time for both linear chains and rings with HI in Θ-solvent. The observed scaling is consistent with $\tau_R \sim N^{3/2}$ expected for Zimm dynamics. (c) Longest relaxation times of linear and ring chains with inclusion of EV and HI show the expected result that $3\nu > 3/2$; however, deviations from the theoretical result of $3\nu = 9/5$ are observed, which could be attributed to the slightly attractive L-J potential used in the simulation. (d) Single molecule conformational relaxation time τ_1 scaling as a function of molecular weight for circular DNA molecules of size 25, 45, and 114.8 kbp from Li and co-workers.[9] Data are replotted by considering spatial resolution when tracking projected polymer extension for the smallest molecular weight chains (see text for details). Relaxation times are scaled to a solvent viscosity of 1 cP, and error bars correspond to to standard deviations in the molecular ensemble, and so do not represent true experimental "error".

RESULTS AND DISCUSSION

Ring Polymer Relaxation. Polymer relaxation is considered for both linear and ring polymers in the presence and absence of hydrodynamic interactions (HI) and excluded volume (EV). We seek to determine the relaxation time of these polymers in order to establish *consistency* between our results and known theoretical scaling results as well as the experimental observations in Li et al.[9] We calculate these relaxation times using two different methods: (1) a chain extension−relaxation protocol analogous to the experiments performed by Li et al.[9] and (2) the time correlation function for the equilibrium end-to-end vector. For method 1 we apply an elongational flow above the coil−stretch transition value ($Wi > 0.5$, or $\tilde{\dot{\epsilon}} \approx 0.01-0.05$). Upon relaxation of the stretched polymer back to an equilibrium conformation, we track the overall projected extension Δx in the $x-y$ plane of the polymer as a function of time. This process is performed for 50−100 trajectories, which are subsequently averaged to produce the average relaxation curves. We fit the tail end of the relaxation (less than 20% of the contour length L) to the form $\Delta x^2/L^2 = Ae^{-t/\tau_r} + B$,[38] which yields the longest polymer relaxation time τ_r as equilibrium is approached.[9] Method 2 tracks the projected extension $\Delta x(t)$ as a function of time for an unstretched polymer (in equilibrium). The time correlation of this value $\langle \Delta x(0) \Delta x(t) \rangle = Ae^{-t/\tau_R} + B$ can be similarly fit to an exponential relaxation. The time correlation function is calculated over $50-300\tau_R$. Each relaxation time is calculated using one of these two procedures; in particular, larger values of N use method 2, which is more computationally efficient (all time steps contribute to the average, not just the tail end of the relaxation), while smaller values of N use method 1, which has a clear connection to experiment.

DOI: 10.1021/acs.macromol.5b02357
Macromolecules 2016, 49, 1961−1971

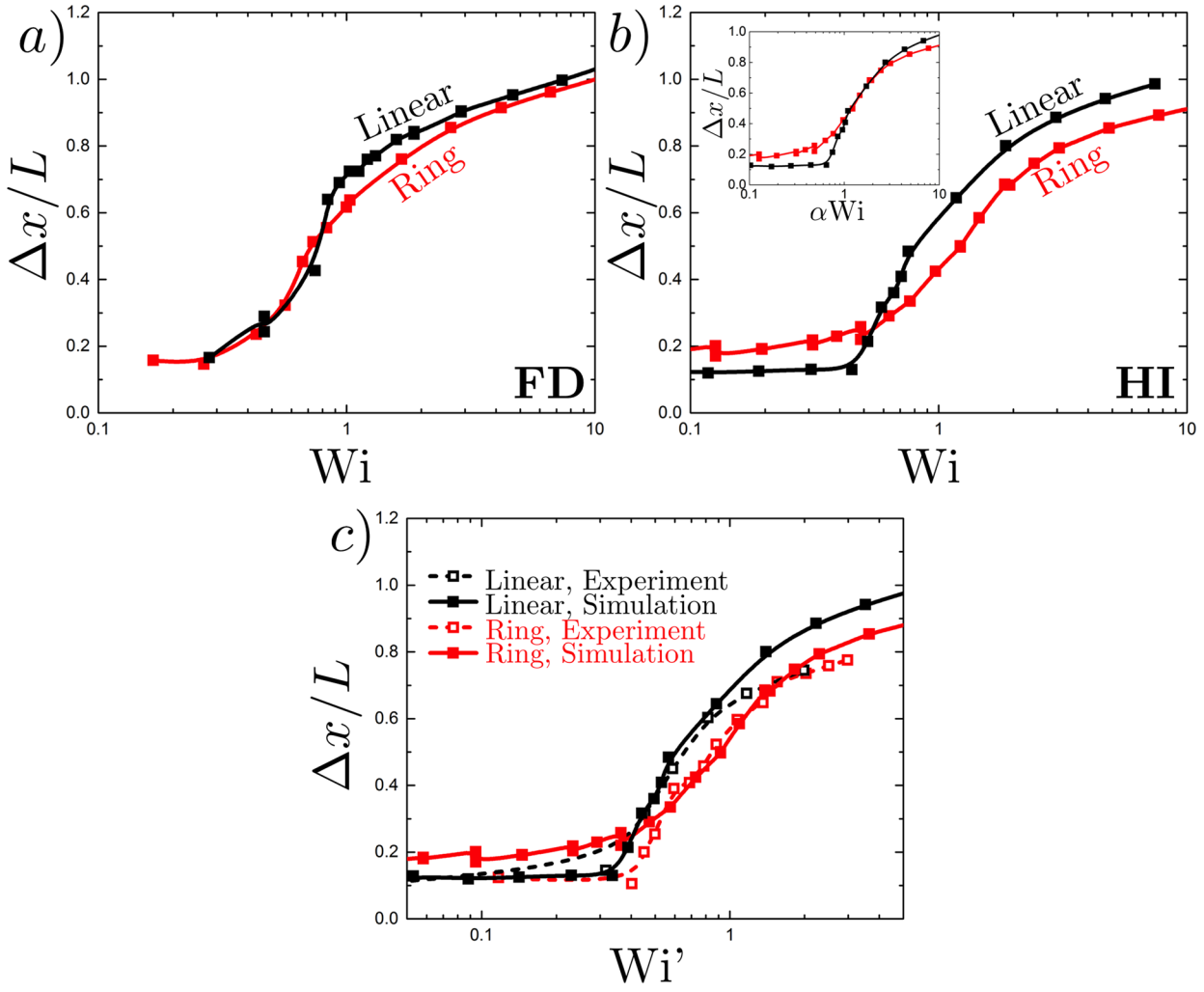

Figure 3. (a) Simulation results for the maximum projected fractional extension $\Delta x/L$ as a function of $Wi = \tilde{\dot{\epsilon}}\tau_R$ for ring (red) and linear chains (black) for the FD case for $N = 120$. Stretching occurs at the same value of Wi for both situations. (b) Simulation results for the maximum projected extension $\Delta x/L$ as a function of Wi upon inclusion of HI leads to a difference between ring and linear chains, with ring polymers stretching at a higher value of Wi. That this effect arises only in the presence of HI *and* ring topologies suggests that the architecture and hydrodynamics couple strongly in this situation. Inset: we can rescale $Wi \rightarrow \alpha Wi$ in a fashion similar to Li et al.[9] If the ring polymer is kept at $\alpha = 1.0$, we obtain a value of $\alpha = 1.45$ for the linear polymer, which is similar to the literature results. (c) Direct comparison of simulation results to single molecule experimental data. Results from Li et al.[9] demonstrate a different stretching transition for ring and linear chains. Experiment and simulation results match for both rings and linear chains when the simulation plots are rescaled by $Wi' = 0.75Wi$, which we attribute to model coarse-graining (see text). $N = 120$, Θ-conditions ($\tilde{u} = 0.35$) for all plots.

Figure 2 shows the relaxation time of both chains and rings at several different values of N. Figure 2a uses the freely draining approximation (FD), and Figure 2b incorporates HI, both in the case of Θ-solvent conditions. The chain length scaling can be directly compared to theoretical predictions.[12,13,38] For the FD case, the linear chain is predicted to exhibit the Rouse dynamics scaling $\tau_R \sim N^2$,[12,38] which is observed in our simulation. The ring polymer similarly scales as $\tau_R \sim N^2$, which is also expected from Rouse dynamics arguments.[12,38,39] For the HI case, the scaling is $\tau_R \sim N^{3/2}$ for both the linear chains and ring chains.[13,38] This follows from the equilibrium structure of these polymer structures. The dynamical scaling predictions for polymers in the Zimm model can be straightforwardly derived:[3,13,38]

$$\tau_R \sim \frac{\langle R_G^2 \rangle}{D} \sim \frac{\eta \langle R_G^2 \rangle^{3/2}}{k_B T} \sim \frac{\eta a^3}{k_B T} N^{3\nu} \quad (5)$$

For both the ideal chain and ring, the exponent $\nu = 0.5$ for Θ-solvent conditions, leading to the $\tau_R \sim N^{3/2}$ result that is corroborated by the simulation.[39,40]

We next studied the relaxation of linear and ring polymers with HI in the presence of excluded volume (EV) interactions. Here, we verify that the inclusion of intrachain EV leads to similar scalings $\tau_R \sim N^{3\nu}$ for both ring and linear polymers. Instead of the value of $\tilde{u} = 0.35$ corresponding to the Θ-condition, where bead attraction counteracts excluded volume, we use now a value of $\tilde{u} = 0.1$, which decreases the attractive portion of the L-J potential such that excluded volume is more pronounced.[28] Figure 2c shows the relaxation times for both rings and linear chains in the presence of EV and HI as a function of chain length, and the expected scaling of $\nu > 0.5$ is observed. In particular, we find a scaling of $\tau_R \sim N^{1.93}$ for the linear case and $\tau_R \sim N^{1.65}$ for the ring case. These results deviate slightly from the expected value of $\tau_R \sim N^{1.8}$, which could arise due to the remaining attractive portion of the L-J pair potential

DOI: 10.1021/acs.macromol.5b02357
Macromolecules 2016, 49, 1961−1971

or (for the linear case) errors in the high-N data points that require long time averages.

For both the FD and HI case, chain relaxation occurs more rapidly for the ring polymer. This can be understood due to the differences in the mode structure; the ring boundary conditions do not permit the lowest mode that exists in the chain Rouse motion, and instead the lowest mode has half the wavelength ($\lambda_{1,\mathrm{Chain}} = 2\lambda_{1,\mathrm{Ring}}$). This mode relaxes more quickly, in principle by a factor of 4 for the non-HI case ($\tau_1 \sim 1/\lambda_1^2$).[12,38] This prediction is consistent with the factor between the ring and linear cases in FD, which is approximately $\tau_{\mathrm{R,Chain}}/\tau_{\mathrm{R,Ring}} \approx 4$. Predictions of $\tau_{\mathrm{R,Chain}}/\tau_{\mathrm{R,Ring}}$ for the HI case have been determined using a number of explicit solvent simulation methods (such as lattice Boltzmann and stochastic rotation dynamics).[41] Fully repulsive potentials are known to exhibit a smaller-than-FD ratio $\tau_{\mathrm{R,Chain}}/\tau_{\mathrm{R,Ring}} \approx 1.1$. This is qualitatively consistent with our observations of a similar decrease in $\tau_{\mathrm{R,Chain}}/\tau_{\mathrm{R,Ring}}$ as excluded volume is included.

We can further compare our simulation results for ring polymer relaxation to recent single molecule experimental results. Similar scalings for center-of-mass diffusion coefficients D have been observed for ring and linear chains based on single molecule translational diffusion experiments.[42] In particular, single chain diffusion measurements revealed similar power-law scalings for the diffusion coefficients of linear DNA ($D_{\mathrm{L}} \sim L^{-0.59}$) and circular DNA ($D_{\mathrm{C}} \sim L^{-0.57}$).[42] In principle, single chain diffusion measurements can be directly compared to conformation chain relaxation measurements, provided that the latter is observed at the tail end of the relaxation (i.e., at small extensions), which is the method that we employ here.[38] In addition, recent single molecule experiments by Li and co-workers report longest polymer relaxation times for rings measured directly from conformation relaxation.[9] In Figure 2d, we replot the experimental data from Li et al.[9] with two minor modifications. First, for the smallest molecular weight circular chains (25 kbp), we fit the terminal 50% ($x/L < 0.5$) of the conformational relaxation trajectory to a double-exponential function, and we take the longest time constant as the longest polymer relaxation time τ_1. The shorter exponential accounts for higher-order Rouse mode(s) that are expected to be non-negligible when more of the chain relaxation is fit, which is important when it is difficult to resolve only the tail end of the chain relaxation for small molecules.[38] For all other cases (linear and circular), we use the standard method of fitting the terminal 30% to a single-exponential decay. For the smallest molecular weight chains (25 kbp), this method provides a more accurate estimate for τ_1 due to experimental error in visual tracking of projected polymer extension near the coiled state, which begins to approach the diffraction limit for these polymers. Second, we include error bars in Figure 2d that correspond to standard deviations in the molecular ensemble arising from individual relaxation trajectories. Using this method, the single molecule conformational relaxation data for ring polymers are in good agreement with the BD simulation results for ring polymer with HI and EV. Finally, we note that recent computational results that consider the semiflexible nature of double-stranded DNA suggest that backbone flexibility (or inflexibility) gives rise to a slightly lower excluded volume exponent $\nu_{\mathrm{eff}} \approx 0.54$, even in the context of athermal solvents.[43] These results appear to agree with our experimental data.

Coil−Stretch Transition in Elongational Flow. We further investigated the nonequilibrium stretching dynamics of single ring polymers in a planar elongational flow. Experimental results suggest that the coil−stretch transition is noticeably different between the linear and ring architectures,[9] with the ring stretching at a higher dimensionless flow strength or Weissenberg number than the linear polymer consistently for any value of N. To study polymer chain stretching, we determine the steady-state elongation Δx in the elongational flow stretching axis at a given value of $\tilde{\dot{\epsilon}}$. We normalize this value of the flow strength with the relaxation time of the polymer to calculate the Weissenberg number $Wi = \tilde{\dot{\epsilon}}\tilde{\tau}_{\mathrm{R}}$.

Figure 3a plots the fractional projected extension $\Delta x/L$ of a polymer for the FD case. Both rings and chains are studied here, with the contour length L of the ring polymer equal to half of the contour length of the linear counterpart $L_{\mathrm{ring}} = L_{\mathrm{lin}}/2$. Plotted against Wi, for $N = 120$ the coil−stretch transition of the ring occurs at essentially the same value as the linear chain for the FD case. Figure 3b plots the elongation versus Wi upon inclusion of HI. In this case, a difference is observed between the two architectures, with the coil−stretch transition occurring at higher values of Wi for ring polymers. This is apparent in both simulation and experiment, which demonstrate almost exact matching when plotted together in Figure 3c. Excellent agreement between experiments and simulation for steady-state fractional extension for linear and ring chains is observed when the Wi of the simulation results is rescaled by a small constant value $Wi' = 0.75Wi$, which may be attributed to the coarse-grained representation of the stretching DNA in the experiment. Apparent differences in experimental and computational results occur at high flow rates, which is likely due to the use of a bead−rod model that does not display Marko−Siggia force−extension behavior in the high flow rate limit.[44] Nevertheless, the agreement between the experiments and simulations for two different chain architectures suggests that the model is capturing the correct physics. Interestingly, the difference between the coil−stretch transition for the ring and linear chains only exists upon inclusion of HI, indicating that the difference is driven largely by hydrodynamic effects. In an absolute sense, the polymer chain relaxation is much faster for rings due to the changes in mode structure; however, this difference is taken out of consideration when Wi is used due to its normalization by the longest relaxation time scale. Therefore, additional physics must be responsible that are not captured in the equilibrium relaxation time of the hydrodynamic interacting ring polymer.

We hypothesize an explanation for the observed shift in the coil−stretch transition that stems from intramolecular HI. In the equilibrium conformation, a monomer in a ring polymer sees an environment where HI is largely screened. This changes, however, as the polymer starts to stretch. Chain stretching affects the conformation by dragging the monomers away from the center of mass along the x coordinate (direction of the principal axis of extension). However, each monomer that moves in this direction must correspond to another monomer that moves the chain in the same direction such that the ring constraint is maintained. This is seen in highly stretched conformations as the two stretched portions of the ring. In some sense, two polymers that are connected at the extreme values of x are being stretched simultaneously, and they also hydrodynamically couple as shown in the schematic in Figure 4a. In the absence of HI, the fluid flow exerts a force $\tilde{f}_{\mathrm{Flow}}$ on a given chain monomer that is directly related to its position. An entropic restoring force $\tilde{f}_{\mathrm{S}}$ pulls this monomer in the other

DOI: 10.1021/acs.macromol.5b02357
Macromolecules 2016, 49, 1961−1971

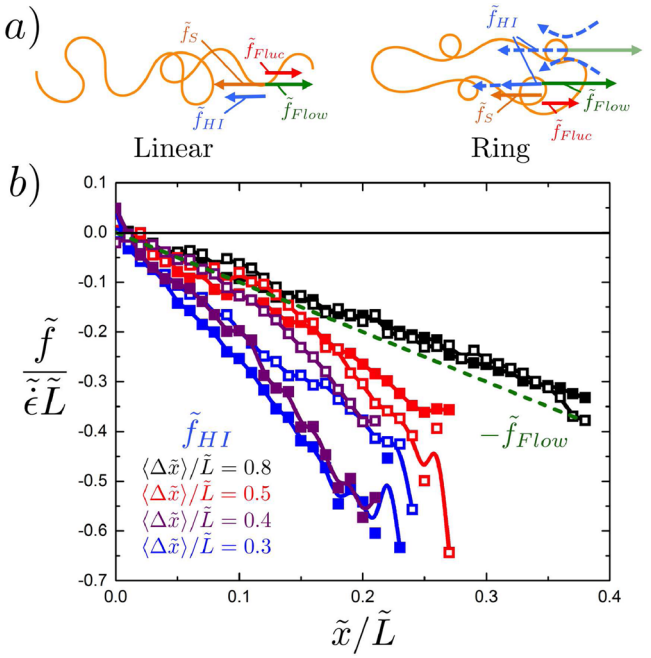

Figure 4. The presence of the ring constraint leads to cooperative chain relaxation that shifts the location of the coil−stretch transition. (a) Schematic demonstrating the forces on a slightly stretched linear polymer and on a slightly stretched ring polymer. In both the ring and the linear polymer, forces such as the Brownian force $\tilde{f}_B$ and entropic spring force $\tilde{f}_S$ remain essentially the same. In contrast, the hydrodynamic force $\tilde{f}_{HI}$ is stronger in the ring, where two stretching portions of the ring polymer exert a backflow felt by each other. A stronger applied fluid flow $\tilde{f}_{Flow}$ is thus required to maintain the same stretch. (b) Calculations of the hydrodynamic forces $\tilde{f}_{HI}$ (connected symbols) on stretching polymers in simulation demonstrate this effect. At intermediate stretching ($\Delta x/L \approx 0.3$–0.4), the hydrodynamic forces are stronger for the ring polymer (closed symbols) than the linear polymer (open symbols). As the polymer is stretched, the backflow forces approach the point at which they simply cancel out the applied flow (and fall along the $-\tilde{f}_{Flow}$ line, dotted red). For comparison, forces are normalized by the maximum flow force felt by the polymer $\sim\tilde{\dot{\epsilon}}\tilde{L}$ and distances are normalized by the maximum extension length $\tilde{L}$.

direction, a fluctuation force $\tilde{f}_{Fluc}$ that in equilibrium corresponds to Rouse/Zimm motions drives the system to extend, and the sum of these must exactly match the fluid flow force in steady state. This is the case for both linear and ring polymers without HI. When HI is included, there is a disturbance velocity or force on a given bead i due to the hydrodynamic forces on all other beads j. The fluid velocity at the position of bead i, $\mathbf{v}_i$ due to a point force at position j, $\mathbf{f}_j$ is given by the Oseen tensor:

$$\mathbf{v}_i = \frac{1}{8\pi\eta r_{ij}}\left[\mathbf{I} + \frac{\mathbf{r}_{ij}\mathbf{r}_{ij}}{r_{ij}^2}\right]\mathbf{f}_j \tag{6}$$

The velocity at point i is related to the force on a bead of radius a at that same point due to the Stokes friction, $6\pi\eta a\mathbf{v}_i = \mathbf{f}_i$, and therefore the force on a bead at point j exerts a force on the bead at point i via the relationship

$$\tilde{\mathbf{f}}_i = \frac{3}{4\tilde{r}_{ij}}\left[\mathbf{I} + \frac{\tilde{\mathbf{r}}_{ij}\tilde{\mathbf{r}}_{ij}}{\tilde{r}_{ij}^2}\right]\tilde{\mathbf{f}}_j \tag{7}$$

now written in dimensionless form. We can thus define a hydrodynamic force on the chain at a given spatial position $f_{HI}(\tilde{r}_x)$ along the principal axis of extension x:

$$\tilde{f}_{HI}(\tilde{r}_x) = \sum_i \hat{\mathbf{e}}_x \cdot \left[\sum_j \frac{3}{4\tilde{r}_{ij}}\left(\mathbf{I} + \frac{\tilde{\mathbf{r}}_{ij}\tilde{r}_{ij}}{\tilde{\mathbf{r}}_{ij}^2}\right)\tilde{\mathbf{f}}_j\right]\delta(\tilde{r}_{i,x} - \tilde{r}_x) \tag{8}$$

where $\hat{\mathbf{e}}_x$ is the unit vector in the x-direction. Perhaps not surprisingly, for the linear chain in the presence of HI, $\tilde{f}_{HI}$ manifests as a restoring force (Figure 4a, left).

In the context of ring polymers, the presence of HI becomes important due to the proximity of the two, coupled and stretched segments (Figure 4a, right). Each segment exerts this "backflow" on both themselves as well as the other segment, resulting in an additional force orthogonal to the chain stretching direction. To maintain the same fractional chain extension as in the absence of HI, the flow strength must be increased to counter this cooperative relaxation. To account for this relationship, we note that the force on a bead j is proportional to the flow strength ($\tilde{f}_{j,Flow} \sim \tilde{\dot{\epsilon}}$). This force exerts a backflow on neighboring segments, given by an f_{HI} that is similarly proportional to the flow strength ($\tilde{f}_{HI} \sim \phi\tilde{\dot{\epsilon}}$). We have introduced $\phi = \tilde{f}_{HI}/\tilde{f}_{Flow}$, which is a proportionality constant between the force applied on a bead and the effect of its hydrodynamic force on a neighboring strand. Importantly, we can use this hydrodynamic cooperativity to explain the shift in the stretch transition for a ring versus a linear chain. If the flow strength required to stretch a ring polymer in the absence of HI is $\tilde{f}_{Flow,0} \sim \tilde{\dot{\epsilon}}_0$, then the addition of a hydrodynamic restoring force due to a neighboring chain $\tilde{f}_{HI} \sim \tilde{\dot{\epsilon}}$ will require a stronger flow force $\tilde{f}_{Flow} \sim \tilde{\dot{\epsilon}} > \tilde{f}_{Flow,0}$ to maintain the same equilibrium stretch when compared to the FD case. For the same extension, we can write the equation $\tilde{f}_{Flow,0} \sim \tilde{f}_{Flow} + \tilde{f}_{HI}$. We can thus write the equation

$$\tilde{\dot{\epsilon}}^* \sim \frac{\tilde{\dot{\epsilon}}_0^*}{1-\phi} \tag{9}$$

where the value $\tilde{\dot{\epsilon}}^*$ is the flow rate where the coil−stretch transition occurs when there is the nearby stretching strand and $\tilde{\dot{\epsilon}}_0^*$ is the bare coil−stretch transition for the noninteracting strand. Of course, the precise value of the shift depends on the value of $\phi = \tilde{f}_{Flow}/\tilde{f}_{HI}$, which is a proportionality constant that relates the force of the flow on a stretched polymer segment $\tilde{f}_{Flow,i}$ to the force that that segment then exerts on a neighboring stretched segment $\tilde{f}_{HI,j}$. We can provide a rough estimate of this value by taking both forces to be along the primary extensional axis, which leads to an approximate relationship obtained via eq 7:[38]

$$\tilde{f}_{HI,j} = \frac{3}{4\tilde{r}}[1 + \Delta x^2]\tilde{f}_{flow,i} \tag{10}$$

Consider the case where only the closest segments of the neighboring chains lead to dominant interactions. Here, we can make the approximation that the distance $\tilde{r}$ between neighboring segments is of order unity. Furthermore, we are only considering nearest-neighbor interactions between monomers on the two nearby chain segments; these monomers are located at roughly the same x position, so $\Delta x = 0$. If we

DOI: 10.1021/acs.macromol.5b02357
Macromolecules 2016, 49, 1961−1971

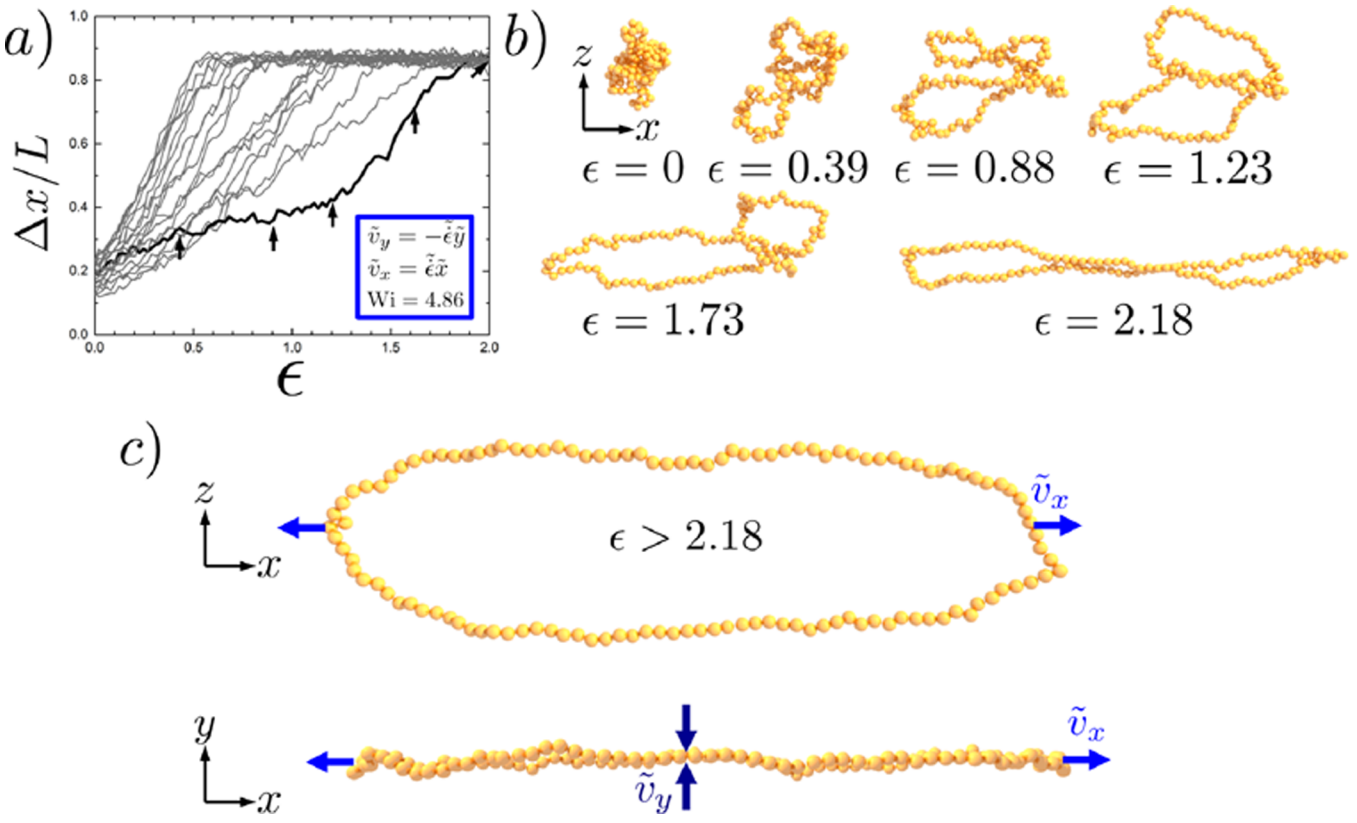

Figure 5. (a) Ring extension $\Delta x/L$ as a function of strain $\epsilon = \tilde{\dot{\epsilon}}\tilde{\tau}_R$ at Wi = 4.86. Stretching of a ring molecule often proceeds unhindered. Occasionally, however, ring stretching can become temporarily trapped as shown in the highlighted trajectory. Arrows denote snapshots, shown in (b), of the hairpin conformation that drives this slow unfolding. Furthermore, looping in the $\tilde{z}$ direction is observed when HI is present ($\epsilon \geq 1.23$). We hypothesize that previous observations of transiently hindered molecular conformations are due to this conformation.[9] (c) At full extension, a large loop is formed in the x−z plane that is absent in the x−y plane. The y−x plane is typically observed in experiment and includes the compressive axis of the flow field $\tilde{v}_y$ as indicated in the figure. This figure also denotes the primary extensional axis, $\tilde{v}_x$, in both the x−y and x−z planes.

consider the closest distance that two segments can approach ($\tilde{r}$ = 2), then this leads to a simple relation for ϕ:

$$\phi \sim \frac{3}{8} \tag{11}$$

This simple model yields a constant shift of the effective elongation rate $\alpha = \tilde{\dot{\epsilon}}^*/\tilde{\dot{\epsilon}}_0^* \approx 1/(1 - 3/8) = 1.6$. Despite the approximations used in this simple model, this shift in the critical Wi at the coil−stretch transition is similar to what is observed in both our simulations and experiments.[9]

This behavior is directly observed in BD simulations. Figure 4b plots the average hydrodynamic forces $\tilde{f}_{HI}$ (normalized by the maximum extension force $\tilde{\dot{\epsilon}}\tilde{L}$) felt by the chain as a function of the distance from the center of mass $\tilde{x}/\tilde{L}$ (normalized by the chain length $\tilde{L}$). The flow force is $\tilde{f}_{Flow} = \tilde{\dot{\epsilon}}\tilde{x}$, so when the force $\tilde{f}_{Flow}$ is plotted in Figure 4b normalized by $\tilde{\dot{\epsilon}}\tilde{L}$, both axes are in terms of $\tilde{x}/\tilde{L}$ and the flow force is plotted independent of $\tilde{\dot{\epsilon}}$. This normalization thus ensures that both topologies and all values of Wi have directly comparable flow forces $\tilde{f}_{Flow}$. Values for $\tilde{f}_{HI}$ are calculated from eq 8 at steady state for both linear (open symbols) and ring (filled symbols) polymers at the same relative extensions $\langle\Delta\tilde{x}\rangle/\tilde{L}$. For low to intermediate extensions $\langle\Delta\tilde{x}\rangle/\tilde{L}$, the difference between the ring and the linear chains is pronounced. At the same extension, the hydrodynamic force on the ring polymer is significantly larger, representing a strong hydrodynamic force driving the molecule toward a relaxed state. This is true relative to the applied flow rate $-\tilde{f}_{Flow}$, denoted by the dotted green line. The local density of stretching "chains" of the ring polymer is low at high extensions, so the HI force for the ring matches with the result for the linear chain. This $\tilde{f}_{HI}$ balances completely with the flow force $\tilde{f}_{Flow}$, as demonstrated by the matching with the dotted green line $-\tilde{f}_{Flow}$ in Figure 4b, and is just a manifestation of the no-net-flow boundary condition at the chain.

Molecular Individualism. One of the key features evident in early investigations of single polymer dynamics was the appearance of molecular individualism.[17,45,46] This corresponds to the variety of different molecular stretching pathways and trajectories that are observed under the same set of flow conditions, even for the same polymer chain under different realizations.[45] Elongational flows yield a wide variety of molecular conformations, such as dumbbell, half-dumbbell, and hairpin topologies.[45] These conformations exhibit different trajectories throughout the coil−stretch transition, with (for example) hairpins taking an extended period of time or a larger accumulated strain to unravel.[45] Alternatively, collapsed molecules in poor solvents typically stretch through a well-defined pathway;[30] however, the presence of knots has been reported for some of these conditions.[32,33] Experimental observations of ring stretching have suggested the possibility of transiently hindered topological states,[9] signified by the presence of fluorescent "spots" near the center of a stretching molecule that leads to long-lasting intermediate states that eventually unravel to the fully extended state.[9]

DOI: 10.1021/acs.macromol.5b02357
Macromolecules 2016, 49, 1961−1971

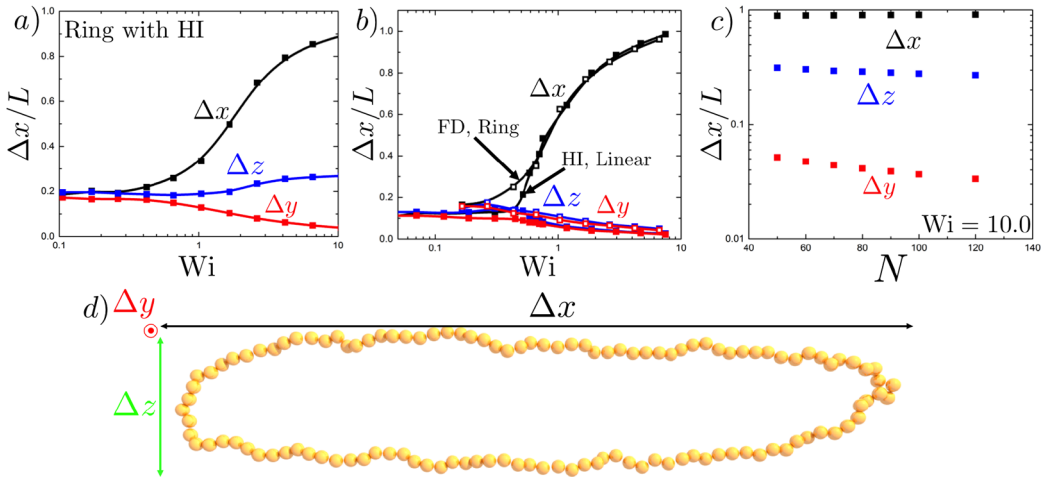

Figure 6. (a) Extension versus *Wi* for a ring polymer with HI (N = 120). The primary extension direction of the flow is Δx, and the compression direction of the flow is Δy. HI and the ring topology lead to stretching in the Δz-direction above the coil−stretch transition, leading to a *looped* conformation. (b) Extension versus *Wi* for a ring polymer without HI (FD, open symbols) and for a linear polymer with HI (filled symbols). In contrast to (a), stretching only happens in the Δx-direction, and both Δy and Δz decrease above the coil−stretch transition. Both HI and ring topologies are needed to observe looping conformations. (c) Fraction extension $\Delta x/L$ as a function of N (*Wi* = 10.0), demonstrating that Δx and Δz scale roughly linearly with N. The ratio of the length and width of the loop is therefore roughly constant. (d) Simulation snapshot of a loop conformation, indicating the dimensions considered in (a−c).

We characterize the stretching of ring polymers directly from simulation, and we quantify this in terms of the transient fractional $\Delta x/L$ in flow (Figure 5a). Most ring polymers stretch in an unhindered fashion (Figure 5a, light gray trajectories), analogous to the dumbbell conformations observed in linear polymers.[45] Occasionally, however, the extending chains become kinetically trapped the stretching process. This is observed in Figure 5a as a hindered state indicated by a darkened trajectory. The coarse-grained spatial resolution of the simulation permits direct observation of the conformation in this state. Snapshots along this trajectory are shown in Figure 5b as a "hairpin" similar to that seen in linear polymers.[45] If the ring polymer doubles back on itself, which happens far less frequently due to the looping constraint, then the chain is trapped in a state that may persist for large amounts of accumulated fluid strain. In Figure 5b, the ring polymer appears to occupy a large spatial dimension in the nonflow (z) direction, which is apparent for strains $\epsilon \geq 1$. This "bunching up" of internal polymer segments may be responsible for these observations from single molecule experiments despite the presence of a hairpin conformation and leads to large loops at full extension (Figure 5c, $\epsilon > 2.18$). It is apparent that the loop conformation in Figure 5c is transiently observed in the trajectories leading to the fully extended conformation (Figure 5b, ϵ = 0.88, 1.23, 1.73). The breakup of these loops, which requires nonlooped conformations (Figure 5b, ϵ = 2.18), may lead to "stuck" conformations along the stretching trajectory such as those observed in Figure 5a and Li et al.[9]

Chain Looping. Planar extensional flow is described by a principal axis of extension (x-direction) and an orthogonal principal axis of compression (y-direction). In this flow, the third direction (z-direction) is stagnant with no imposed fluid flow. Interestingly, for ring polymers in a planar extension flow, we observe a large degree of polymer stretch in the z-direction, which is consistently found in our simulations over a wide range of flow conditions. It is intuitive to consider a stretched ring that primarily extends only in the flow direction at the expense of stretching in the orthogonal dimensions. This is certainly the case for linear chains at high stretching dimensions;[44,47] however, this does not appear to be the case for stretched ring polymers in a planar extensional flow. A "loop" conformation is observed in simulation snapshots shown in Figure 5c, which is characterized by a large amount of stretching in the z-direction that is concomitant with stretching in the x-direction (the principal axis of extension) due to the applied elongational fluid flow. Chain looping and exaggerated chain stretch only occur in the z-direction, rather than the y-direction (the principal axis of compression) where the applied fluid flow drives the polymer toward its center of mass in that coordinate.

This looping behavior is a marked example of the coupling between HI and chain topology. We demonstrate this by tracking chain dimensions in all three dimensions across the coil−stretch transition. For a ring polymer with HI, we plot the dimensions $\Delta x/L$, $\Delta y/L$, and $\Delta z/L$ as a function of *Wi* (Figure 6a). The extension of the chain Δx in the principal axis of extension is accompanied by a similar increase in the chain dimension in the z-direction. This contrasts with the stretching behavior when HI is removed (Figure 6b, open symbols) or the chain is linear (Figure 6b, closed symbols). Upon removing either one of these aspects, Δz decreases for flow strengths above the coil−stretch transition.

We quantify the geometry of the looped conformation as the contour length of the ring polymer is increased from N = 50 to N = 120 (Figure 6c). At an intermediate to large flow rate *Wi* = 10.0, we measure the normalized extension of the ring along the stretching direction $\Delta x/L$ as well as the extension of the ring along the z-direction $\Delta z/L$. We also plot the extension in the y-direction, which as expected becomes small.[44] In the $\Delta x/L$ direction, the stretching is consistently significantly less than the maximum due to the large extension of $\Delta z/L$. The ratio of these two $\Delta x/\Delta z$ remains essentially constant at all values of N. A snapshot of an extended ring is shown in Figure 6d, demonstrating the various dimensions and the nearly constant ratio of $\Delta x/\Delta z \approx 4$.

DOI: 10.1021/acs.macromol.5b02357
Macromolecules 2016, 49, 1961−1971

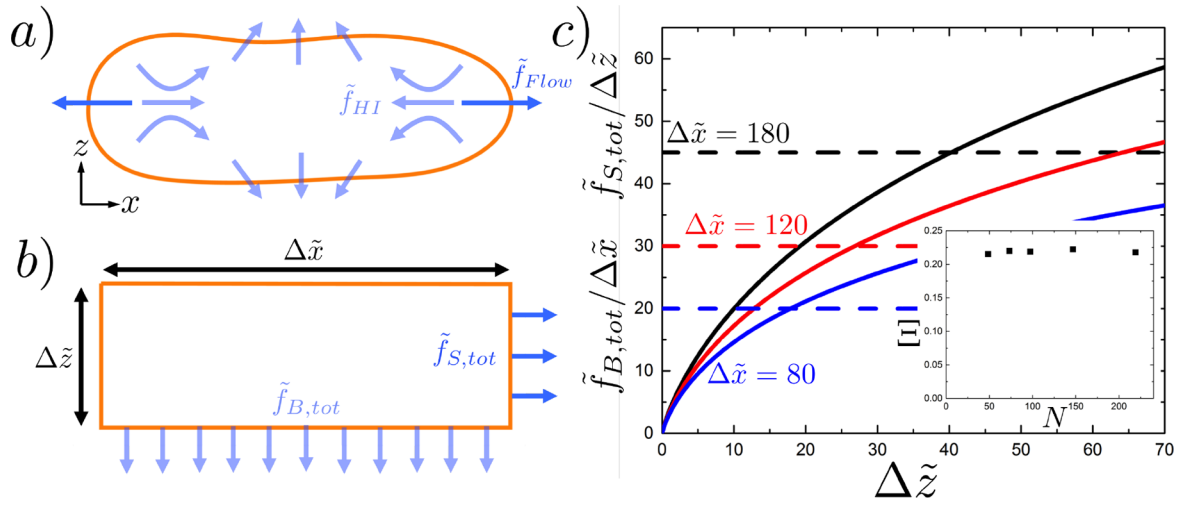

Figure 7. (a) Schematic demonstrating how loop conformations arise in planar elongational flow. The flow in the x-direction exerts a force $\tilde{f}_{Flow}$ that is counteracted by a backflow due to HI with the corresponding force $\tilde{f}_{HI}$. This flow exerts a flow on the top and bottom of the loop in the z-direction. (b) We approximate the loop conformation as a rectangular loop, with force along the sides $\tilde{f}_{S,tot}$ due to the applied flow and a force along the bottom $\tilde{f}_{B,tot}$ due to the presence of HI. Symmetric forces along the top and left side are present, but not drawn. The dimensions of this rectangular ring are $\Delta\tilde{x}$ in the x-direction and $\Delta\tilde{z}$ in the z-direction. (c) The average force per monomer on the bottom and top ($\tilde{f}_{B,tot}/\Delta\tilde{x}$) and the average force per monomer on the sides ($\tilde{f}_{S,tot}/\Delta\tilde{z}$) are plotted. A number of rectangles are considered, with fixed top and bottom lengths $\Delta\tilde{x}$ as a function of the side lengths $\Delta\tilde{z}$. The condition where the force per distance $\tilde{f}_{B,tot}/\Delta\tilde{x}$ and $\tilde{f}_{S,tot}/\Delta\tilde{z}$ are equal represents the equilibrium dimensions of a fully stretched ring polymer. This intersection can be plotted on a graph of $\Xi = \Delta\tilde{z}/\Delta\tilde{x}$ as a function of $N = \Delta\tilde{x} + \Delta\tilde{z}$ (inset) to demonstrate that the dimensions of the loop are essentially constant.

This behavior can be qualitatively understood via the schematic in Figure 7a. As a polymer is extended by the flow, the stretched chain exerts an opposing force on the fluid. This force propagates via a secondary flow through the solvent, producing a counterflow in the direction of the light blue arrows. In an elongated geometry, there is a net flow in the negative z-direction from the upper and side portions of the ring acting on the lower portion and a net flow in the positive z-direction due to the lower portion and sides of the ring acting on the upper portion. Therefore, these hydrodynamic backflows push the two extended portions of the ring polymer away from each other in the z-direction. A similar hydrodynamic effect has been observed in linear chains near surfaces.[48−56]

We further provide a quantitative argument for these observations on ring polymer looping in flow. From the snapshots of the simulation (Figures 5 and 6), we can approximate the chain conformation as a rectangle with sides of length Δz and Δx in the appropriate directions (Figure 7b). We calculate the forces per monomer of both segments for a given elongational flow rate. As a first approximation, we assume that any given monomer has essentially the same radial force acting upon it. This is essentially the idea that the free energy is minimized because if there is a stronger force on (for example) the z-oriented segment, then an increase in its length at the expense of the x-oriented segment is going to occur as this decreases the overall energy of the system.

To calculate the extent of chain looping, we consider the force on a monomer i ($\tilde{f}_i$) due to an applied force on monomer j ($\tilde{f}_j$). This can be described by the Oseen tensor:[38]

$$\tilde{\mathbf{f}}_i = \frac{3}{4\tilde{r}_{ij}}\left[\mathbf{I} + \frac{\tilde{\mathbf{r}}_{ij}\tilde{\mathbf{r}}_{ij}}{\tilde{r}_{ij}^{\,2}}\right]\tilde{\mathbf{f}}_j \tag{12}$$

To find the total force due to the top (T) of the rectangle (in the x-direction) on the bottom (B) of the rectangle (in the z-direction), we calculate the following integral:

$$\tilde{f}_{\mathrm{TB,tot}} = \frac{3}{4}\int_{-\Delta\tilde{x}/2}^{\Delta\tilde{x}/2} d\tilde{x}_1 \int_{-\Delta\tilde{x}/2}^{\Delta\tilde{x}/2} d\tilde{x}_2\, \tilde{f}_{\mathrm{T}}\left[\frac{\Delta\tilde{z}(\tilde{x}_1 - \tilde{x}_2)}{(\Delta\tilde{z}^2 + (\tilde{x}_1 - \tilde{x}_2)^2)^{3/2}}\right] \tag{13}$$

$$\tilde{f}_{\mathrm{TB,tot}} = -\frac{3\tilde{\epsilon}\Delta\tilde{z}}{8}\left[4(\Delta\tilde{z} - \sqrt{\Delta\tilde{z}^2 + \Delta\tilde{x}^2}) + \Delta\tilde{x} \times \ln\left(\frac{\sqrt{\Delta\tilde{z}^2 + \Delta\tilde{x}^2} + \Delta\tilde{x}}{\sqrt{\Delta\tilde{z}^2 + \Delta\tilde{x}^2} - \Delta\tilde{x}}\right)\right] \tag{14}$$

where $\tilde{f}_{\mathrm{T}} = -\tilde{\epsilon}\tilde{x}_1$ is the force of the chain on the surrounding fluid. Likewise, the side of the rectangle has a similar effect on the bottom of the rectangle:

$$\tilde{f}_{\mathrm{SB,tot}} = \frac{3}{2}\int_0^{-\Delta\tilde{x}} d\tilde{x} \int_0^{\Delta\tilde{z}} d\tilde{z}\, \tilde{f}_{\mathrm{S}}\left[\frac{\tilde{z}\tilde{x}}{(\tilde{x}^2 + \tilde{z}^2)^{3/2}}\right] \tag{15}$$

$$\tilde{f}_{\mathrm{SB,tot}} = \frac{3\tilde{\epsilon}\Delta\tilde{x}}{4}[\sqrt{\Delta\tilde{x}^2 + \Delta\tilde{z}^2} - \Delta\tilde{x} - \Delta\tilde{z}] \tag{16}$$

where $\tilde{f}_{\mathrm{S}} = -\tilde{\epsilon}\Delta\tilde{x}/2$ is the force of the sides on the surrounding fluid. There is a factor of 2 difference between the prefactor for this and $\tilde{f}_{\mathrm{TB,tot}}$ due to the inclusion of both sides. The total force on the bottom of the loop is $\tilde{f}_{\mathrm{B,tot}} = \tilde{f}_{\mathrm{TB,tot}} + \tilde{f}_{\mathrm{SB,tot}}$. The side of the rectangle feels a force primarily due to the applied fluid flow, $\tilde{f}_{\mathrm{S,tot}} = \tilde{\epsilon}\Delta\tilde{x}\Delta\tilde{z}/4$.

Figure 7c plots $\tilde{f}_{\mathrm{B,tot}}/\Delta\tilde{x}$ and $\tilde{f}_{S,tot}/\Delta\tilde{z}$ as a function of $\Delta\tilde{z}$ for a number of values $\Delta\tilde{x}$. The point at which both values intersect roughly represents a steady-state situation (i.e., the force per distance along all edges of the rectangle are equivalent). The ratio of $\Xi = \Delta\tilde{z}/\Delta\tilde{x}$ at which this occurs is plotted in the inset of Figure 7c as a function of the total chain length $N = \Delta\tilde{x} + \Delta\tilde{z}$. At all values of N considered here, this calculation

DOI: 10.1021/acs.macromol.5b02357
Macromolecules 2016, 49, 1961−1971

demonstrates that the geometry converges on a value of $\Xi \approx 0.22$, which is essentially independent of N and $\tilde{\dot{\epsilon}}$. This corresponds to the simulation results in Figure 6, which are in near-quantitative agreement with this result. We expect that deviations from this theoretical result could be associated with the approximation of the loop as a rectangle, which limits this result to regimes well above the coil−stretch transition where the ring is strongly stretched.

CONCLUSIONS

Ring polymers represent a model architecture that provides insight into the effect of topological constraints on their dynamics. While a great deal of prior work has focused on melt rheology,[1,4−8] we demonstrate that nontrivial effects emerge even in dilute solution. Our work provides a physical basis for understanding many of the single molecule experimental results of Li et al.[9] and provides new insight into the ways that polymer topology and hydrodynamic interactions couple. In particular, there are two effects that emerge from the ring architecture: the hydrodynamic perturbation of the coil−stretch transition and the large looping behavior of rings in flow. Indeed, these effects are apparent only in highly out-of-equilibrium scenarios, whereas equilibrium chain dynamics (i.e., relaxation times) experience minor deviations from standard linear chain dynamics.[12,13,38,39] We attribute both the shift in the coil−stretch transition and the looping behavior to the ring topology and its effect on hydrodynamics, which leads to a coupled backflow that is not present in linear chains. Theoretical arguments support this observation.

We expect the coupling between hydrodynamics and topology to manifest differently in other flows. For example, uniaxial extension will likely demonstrate similar shifts in the coil−stretch transition; however, looping behavior may be suppressed due to the inward flow along both compressional flow directions. Likewise, linear mixed flows may result in interesting combinations of polymer chain tumbling and looping that warrant a promising area of further inquiry. Eventually, an expanded parameter space (e.g., chain flexibility, concentration) will hopefully help inform the broader effort to understand the rheology of ring polymers.

The effects elucidated in this work may provide new opportunities for the manipulation of topologically interesting polymers. Many biomacromolecules possess looped structures, including genomic DNA.[57−59] The ability of elongational flows to drive *looped* conformations may present ways to sort or manipulate both biological and synthetic ring polymers. Furthermore, other topologies (star polymers, dendritic polymers, branched polymers) may demonstrate similar effects. In general, the ability of chain architecture to influence hydrodynamics may present the opportunity to "design in" handles to manipulate single chains, such that branches or looped sections can be included to dictate single-chain dynamics. This behavior may also inform the behavior of single chains in nondilute systems. In some sense, a stretched ring polymer is similar to two linear polymers stretching in close proximity; based on our results, it is possible that new and interesting hydrodynamic effects may also arise if this condition is imposed by high local polymer concentrations rather than chain connectivity.

AUTHOR INFORMATION

Corresponding Author

*E-mail: cesing@illinois.edu (C.E.S.).

Notes

The authors declare no competing financial interest.

ACKNOWLEDGMENTS

The authors thank Greg McKenna and Yanfei Li for useful discussions. This work was funded by a Dow Chemical Graduate Fellowship for K.-W.H. and the David and Lucile Packard Foundation, NSF CAREER Award CBET-1254340, and the Camille and Henry Dreyfus Foundation for C.M.S.

REFERENCES

(1) McLeish, T. Polymers Without Beginning or End. *Science* **2002**, *297*, 2005−2006.
(2) De Gennes, P. G. *Scaling Concepts in Polymer Physics*; Cornell University Press: Ithaca, NY, 1979.
(3) Rubinstein, M.; Colby, R. *Polymer Physics*; Oxford University Press: Oxford, UK, 2003.
(4) Kapnistos, M.; Lang, M.; Vlassopoulos, D.; Pyckhout-Hintzen, W.; Richter, D.; Cho, D.; Chang, T.; Rubinstein, M. Unexpected Power-Law Stress Relaxation of Entangled Ring Polymers. *Nat. Mater.* **2008**, *7*, 997−1002.
(5) Halverson, J. D.; Lee, W. B.; Grest, G. S.; Grosberg, A. Y.; Kremer, K. Molecular Dynamics Simulation Study of Nonconcatenated Ring Polymers in a Melt. I. Statics. *J. Chem. Phys.* **2011**, *134*, 204904.
(6) Halverson, J. D.; Grest, G. S.; Grosberg, A. Y.; Kremer, K. Rheology of Ring Polymer Melts: From Linear Contaminants to Ring-Linear Blends. *Phys. Rev. Lett.* **2012**, *108*, 038301.
(7) Robertson, R. M.; Smith, D. E. Strong Effects of Molecular Topology on Diffusion of Entangled DNA Molecules. *Proc. Natl. Acad. Sci. U. S. A.* **2007**, *104*, 4824−4827.
(8) Muller, M.; Wittmer, J. P.; Cates, M. E. Topological Effects in Ring Polymers: A Computer Simulation Study. *Phys. Rev. E: Stat. Phys., Plasmas, Fluids, Relat. Interdiscip. Top.* **1996**, *53*, 5063−5074.
(9) Li, Y.; Hsiao, K.-W.; Brockman, C. A.; Yates, D. Y.; Robertson-Anderson, R. M.; Kornfield, J. A.; San Francisco, M. J.; Schroeder, C. M.; McKenna, G. B. When Ends Meet: Circular DNA Stretches Differently in Elongational Flows. *Macromolecules* **2015**, *48*, 5997−6001.
(10) Marciel, A. B.; Mai, D. J.; Schroeder, C. M. Template-Directed Synthesis of Structurally Defined Branched Polymers. *Macromolecules* **2015**, *48*, 1296−1303.
(11) Marciel, A.; Schroeder, C. M. New Directions in Single Polymer Dynamics. *J. Polym. Sci., Part B: Polym. Phys.* **2013**, *51*, 556−566.
(12) Rouse, P. E. A Theory of the Linear Viscoelastic Properties of Dilute Solutions of Coiling Polymers. *J. Chem. Phys.* **1953**, *21*, 1272−1280.
(13) Zimm, B. H. Dynamics of Polymer Molecules in Dilute Solution: Viscoelasticity, Flow Birefringence and Dielectric Loss. *J. Chem. Phys.* **1956**, *24*, 269−278.
(14) Peterlin, A. Hydrodynamics of Linear Macromolecules. *Pure Appl. Chem.* **1966**, *12*, 563−586.
(15) De Gennes, P. G. Coil-stretch transition of dilute flexible polymers under ultrahigh velocity gradients. *J. Chem. Phys.* **1974**, *60*, 5030−5042.
(16) Schroeder, C. M.; Babcock, H. P.; Shaqfeh, E. S. G.; Chu, S. Observation of Polymer Conformation Hysteresis in Extensional Flow. *Science* **2003**, *301*, 1515−1519.
(17) Larson, R. G. The Rheology of Dilute Solutions of Flexible Polymers: Progress and Problems. *J. Rheol.* **2005**, *49*, 1−70.
(18) Shaqfeh, E. S. G. The Dynamics of Single-Molecule DNA in Flow. *J. Non-Newtonian Fluid Mech.* **2005**, *130*, 1−28.
(19) Smith, D. E.; Perkins, T. T.; Chu, S. Dynamical Scaling of DNA Diffusion and Coefficients. *Macromolecules* **1996**, *29*, 1372−1373.

DOI: 10.1021/acs.macromol.5b02357
Macromolecules 2016, 49, 1961−1971

(20) Perkins, T. T.; Quake, S. R.; Smith, D. E.; Chu, S. Relaxation of a Single DNA Molecule Observed by Optical Microscopy. *Science* **1994**, *264*, 822−823.
(21) Perkins, T. T.; Smith, D. E.; Chu, S. Direct Observation of Tube-Like Motion of a Single Polymer Chain. *Science* **1994**, *264*, 819−822.
(22) Mai, D. J.; Marciel, A. B.; Sing, C. E.; Schroeder, C. M. Topology-Controlled Relaxation Dynamics of Single Branched Polymers. *ACS Macro Lett.* **2015**, *4*, 446−452.
(23) Perkins, T. T.; Smith, D. E.; Larson, R. G.; Chu, S. Stretching of a Single Tethered Polymer in a Uniform Flow. *Science* **1995**, *268*, 83−87.
(24) Smith, D. E.; Babcock, H. P.; Chu, S. Single-Polymer Dynamics in Steady Shear Flow. *Science* **1999**, *283*, 1724−1727.
(25) Hur, J. S.; Shaqfeh, E. S. G.; Larson, R. G. Brownian Dynamics Simulations of Single DNA Molecules in Shear Flow. *J. Rheol.* **2000**, *44*, 713−742.
(26) Schroeder, C. M.; Teixeira, R. E.; Shaqfeh, E. S. G.; Chu, S. Characteristic Periodic Motion of Polymers in Shear Flow. *Phys. Rev. Lett.* **2005**, *95*, 018301.
(27) Resiner, W.; Morton, K. J.; Riehn, R.; Wang, Y. M.; Yu, Z.; Rosen, M.; Sturm, J. C.; Chou, S. Y.; Frey, E.; Austin, R. H. Statics and Dynamics of Single DNA Molecules Confined in Nanochannels. *Phys. Rev. Lett.* **2005**, *94*, 196101.
(28) Alexander-Katz, A.; Netz, R. Dynamics and Instabilities of Collapsed Polymers in Shear Flow. *Macromolecules* **2008**, *41*, 3363−3374.
(29) Alexander-Katz, A.; Schneider, M. F.; Schneider, S. W.; Wixforth, A.; Netz, R. Shear-Flow-Induced Unfolding of Polymeric Globules. *Phys. Rev. Lett.* **2006**, *97*, 138101.
(30) Sing, C. E.; Alexander-Katz, A. Globule-Stretch Transitions of Collapsed Polymers in Elongational Flow Fields. *Macromolecules* **2010**, *43*, 3532−3541.
(31) Sing, C. E.; Alexander-Katz, A. Dynamics of Collapsed Polymers Under the Simultaneous Influence of Elongational and Shear Flows. *J. Chem. Phys.* **2011**, *135*, 014902.
(32) Tang, J.; Du, N.; Doyle, P. S. Compression and Self-Entanglement of Single DNA Molecules Under Uniform Electric Field. *Proc. Natl. Acad. Sci. U. S. A.* **2011**, *108*, 16153−16158.
(33) Dai, L.; Renner, C. B.; Doyle, P. S. Origin of Metastable Knots in Single Flexible Chains. *Phys. Rev. Lett.* **2015**, *114*, 037801.
(34) Lang, P. S.; Obermayer, B.; Frey, E. Dynamics of a Semiflexible Polymer or Ring Shear Flow. *Phys. Rev. E* **2014**, *89*, 022606.
(35) Chen, W.; Li, Y.; Zhao, H.; Liu, L.; Chen, J.; An, L. Conformations and Dynamics of Single Flexible Ring Polymers in Simple Shear Flow. *Polymer* **2015**, *64*, 93−99.
(36) Yamakawa, H. Transport Properties of Polymer Chains in Dilute Solution: Hydrodynamic Interaction. *J. Chem. Phys.* **1970**, *53*, 436−443.
(37) Rotne, J.; Prager, S. Variational Treatment of Hydrodynamic Interaction in Polymers. *J. Chem. Phys.* **1969**, *50*, 4831−4837.
(38) Doi, M.; Edwards, S. F. *The Theory of Polymer Dynamics*; Oxford University Press: Oxford, UK, 1988.
(39) Bloomfield, V.; Zimm, B. H. Viscosity, Sedimentation, et Cetera, of Ring- and Straight-Chain Polymers in Dilute Solution. *J. Chem. Phys.* **1966**, *44*, 315−323.
(40) Zimm, B. H.; Stockmayer, W. H. The Dimensions of Chain Molecules Containing Branches and Rings. *J. Chem. Phys.* **1949**, *17*, 1301−1314.
(41) Hegde, G. A.; Chang, J.; Chen, Y.; Khare, R. Conformation and diffusion behavior of ring polymers in solution: A comparison between molecular dynamics, multiparticle collision dynamics, and lattice Boltzmann simulations. *J. Chem. Phys.* **2011**, *135*, 184901.
(42) Robertson, R. M.; Laib, S.; Smith, D. E. Diffusion of Isolated DNA Molecules: Dependence on Length and Topology. *Proc. Natl. Acad. Sci. U. S. A.* **2006**, *103*, 7310−7314.
(43) Tree, D. R.; Muralidhar, A.; Doyle, P. S.; Dorfman, K. D. Is DNA a Good Model Polymer? *Macromolecules* **2013**, *46*, 8369−8382.
(44) Marko, J. F.; Siggia, E. D. Stretching DNA. *Macromolecules* **1995**, *28*, 8759−8770.
(45) Perkins, T. T.; Smith, D. E.; Chu, S. Single Polymer Dynamics in an Elongational Flow. *Science* **1997**, *276*, 2016−2021.
(46) de Gennes, P. G. Molecular Individualism. *Science* **1997**, *276*, 1999.
(47) Flory, P. J. *Principles of Polymer Chemistry*; Cornell University Press: Ithaca, NY, 1953.
(48) Fang, L.; Hu, H.; Larson, R. G. DNA Configurations and Concentration in Shearing Flow Near a Glass Surface in a Microchannel. *J. Rheol.* **2005**, *49*, 127−138.
(49) Chen, Y. L.; Graham, M. D.; de Pablo, J. J.; Jo, K.; Schwartz, D. C. DNA Molecules in Microfluidic Oscillatory Flow. *Macromolecules* **2005**, *38*, 6680−6687.
(50) Ma, H.; Graham, M. D. Theory of Shear-Induced Migration in Dilute Polymer Solutions Near Solid Boundaries. *Phys. Fluids* **2005**, *17*, 083103.
(51) Jendrejack, R. M.; Dimalanta, E. T.; Schwartz, D. C.; Graham, M. D.; de Pablo, J. J. DNA Dynamics in a Microchannel. *Phys. Rev. Lett.* **2003**, *91*, 038102.
(52) Jendrejack, R. M.; Schwartz, D. C.; de Pablo, J. J.; Graham, M. D. Shear-Induced Migration in Flowing Polymer Solutions: Simulation of Long-Chain DNA in Microchannels. *J. Chem. Phys.* **2004**, *120*, 2513−2529.
(53) Sing, C. E.; Alexander-Katz, A. Non-monotonic Hydrodynamic Lift Force on Highly Extended Polymers Near Surfaces. *Euro. Phys. Lett.* **2011**, *95*, 48001.
(54) Sing, C. E.; Alexander-Katz, A. Theory of tethered polymers in shear flow: The strong stretching limit. *Macromolecules* **2011**, *44*, 9020−9028.
(55) Sendner, C.; Netz, R. R. Shear-induced repulsion of a semiflexible polymer from a wall. *EPL* **2008**, *81*, 54006.
(56) Serr, A.; Sendner, C.; Muller, F.; Einert, T. R.; Netz, R. R. Single-polymer adsorption in shear: Flattening vs. hydrodynamic lift and surface potential corrugation effects. *EPL* **2010**, *92*, 38002.
(57) Rao, S. S. P.; Huntley, M. H.; Durand, N. C.; Stamenova, E. K.; Bochkov, I. D.; Robinson, J. T.; Sanborn, A. L.; Machol, I.; Omer, A. D.; Lander, E. S.; Aiden, E. L. A 3D Map of the Human Genome at Kilobase Resolution Reveals Principles of Chromatin Looping. *Cell* **2014**, *159*, 1665−1680.
(58) Blattner, F. R.; et al. The Complete Genome Sequence of *Escherichia coli* K-12. *Science* **1997**, *277*, 1453−1462.
(59) Fynan, E. F.; Webster, R. G.; Fuller, D. H.; Haynes, J. R.; Santoro, J. C.; Robinson, H. L. DNA Vaccines: Protective Immunizations by Parenteral, Mucosal, and Gene-Gun Inoculations. *Proc. Natl. Acad. Sci. U. S. A.* **1993**, *90*, 11478−11482.

DOI: 10.1021/acs.macromol.5b02357
Macromolecules 2016, 49, 1961−1971